J Porous Mater (2013) 20:81–94
DOI 10.1007/s10934-012-9577-y

Investigation of chromium oxide clusters grafted on SBA-15 using Cr-polycation sol

P. Hari Krishna Charan · G. Ranga Rao

Published online: 29 February 2012
© Springer Science+Business Media, LLC 2012

Abstract A comparative study of chromium oxide clusters grafted on mesoporous silica SBA-15 was carried out using samples synthesized by one-pot, impregnation and Cr-polycation sol grafting methods. The nature of CrO_x species incorporated into SBA-15 by direct hydrothermal one-pot method as well as impregnation of $Cr(NO_3)_3{\cdot}9H_2O$ and Cr-polycation precursors was characterized by XRD, BET isotherms, UV–Vis DRS, FTIR, TGA, O1s XPS, ^{29}Si-MAS NMR, H_2-TPR, NH_3-TPD, SEM and TEM. Powder XRD did not show the presence of Cr_2O_3 in the calcined samples obtained by one-pot method. It, however, shows the rhombohedral clusters of α-Cr_2O_3 dispersed over SBA-15 for CrO_x/SBA-15 samples prepared by impregnation and polycation sol grafting methods. The absorption band at 296 nm, observed for Cr^{3+} in solution, is absent for the aqueous Cr-polycation sol. There is evidence that the presence of chromium precursor in the reaction medium can influence the morphology of SBA-15 as seen in the SEM micrographs. Charge transfer transitions demonstrate the insertion of CrO_x species on SBA-15 matrix synthesized by one-pot method. Cr-polycation grafted SBA-15 sample shows unique vibrational features at 573 and 624 cm^{-1} attributed to extra-framework CrO_x species. The ratio of Cr^{6+}/Cr^{3+} species present in CrO_x/SBA-15 samples depends on the Cr-precursor employed for grafting on SBA-15. One-pot synthesized samples predominantly contain coordinated water (δ_{H-O-H} at 1,635 cm^{-1}) on SBA-15 while impregnated samples show water molecules associated with CrO_x species (δ_{H-O-H} at 1,594 cm^{-1}).

P. Hari Krishna Charan · G. Ranga Rao (✉)
Department of Chemistry, Indian Institute of Technology Madras, Chennai 600 036, India
e-mail: grrao@iitm.ac.in

Keywords Ordered mesoporous silica · Cr-containing SBA-15 · Chromia · UV–Vis DRS · Polycation sol

1 Introduction

Synthesis and application of silica-based hierarchical porous structures, and various mesoporous metal oxides using nonionic block copolymers have been the topics of interest in porous materials chemistry [1–6]. These materials contain highly ordered, large and uniform mesopore structures (2–50 nm diameter) with surface areas greater than 900 m^2/g. Mesoporous silica materials are rich in isolated, germinal and hydrogen bonded surface silanol groups which can be functionalized and used in catalysis, adsorption, separation and biology [2, 4, 5, 7]. The silicate mesoporous structures are often used as templates to design ordered mesoporous carbons and porous metal oxides such as chromia [2, 8] and metal nanowires of $\sim$6 nm diameter [2]. The structures of mesoporous silicates are often directed by the properties of surfactant molecules employed for the synthesis. The nature of liquid crystal template, formed between the organic surfactants and inorganic silicate species by cooperative self-assembly mechanism, determines the pore architecture of the material. Consequently porous materials exhibit narrow pore size distribution, diverse range of pore and cage symmetries and morphologies. Designing the ordered mesoporous materials in a tunable manner with control over pore size, morphology and composition is the task of synthetic inorganic chemistry. Using biodegradable surfactant (Pluronic P123, $PEO_{20}PPO_{70}PEO_{20}$) as a template, 2D hexagonal structured mesoporous silica SBA-15 has been synthesized with good hydrothermal stability, high crystallinity and uniform pores [1, 2].

Highly ordered mesoporous silicates are advantageous in heterogeneous catalysis in terms of mass transfer through large pores, high concentration of active sites due to large surface area, ordered pores acting as nano-reactors and thus reducing the undesirable side reactions. However mesoporous silicates do not exhibit acid–base or redox properties which are often introduced to facilitate catalytic reactions. Modification of mesoporous silicate systems is governed by the nature of application. Incorporation of metal centers [9–11], metal oxides [12–14], acid-base groups [15–17], and organic functional groups [4, 18] have been done by either direct one-pot synthesis (co-condensation) or post synthesis (impregnation/grafting) methods. However, ordered mesoporous solids are advantageous in stabilizing metal or metal-oxide particles as they cannot grow larger than the pore sizes. The method of introducing metal in the silica matrix also influences the activity of the porous material for the intended reactions [17]. The presence of multivalent transition metal cations in the framework can create isolated redox centers. Since the active sites are easily accessible to the reactant and solvent molecules during the reactions, high conversion rates are possible in the pores. Direct synthesis provides uniform distribution and improves the active site accessibilities in heterogeneous catalysts. Hence the incorporation of heteroatom into the silica structure by direct synthesis is more desirable to obtain well dispersed metal species. The acid templating route leads to lowest-energy-surface particle morphologies. Addition of a variety of electrolytes to the highly acidic reaction mixture has recently been shown to modify the macro-morphologies of the SBA-15 materials [19]. Isomorphic substitution of heteroatom via a co-condensation process with silicon species is very difficult since the metal ion will exist as corresponding oxo-species under strong acidic conditions.

Chromium ion in the 3d series has variable oxidation states, coordination numbers and molecular structure. It forms variety of molecular species in aqueous media and on oxide surfaces depending on the pH and chemical environment [20]. Supported chromium oxide catalysts are widely used in various chemical reactions, such as dehydrogenation of hydrocarbons [20, 21], selective catalytic reduction of nitrous oxide [3] and oxidation of organic compounds [22, 23]. Silica and SBA-15 supported Cr_2O_3 have been studied for ethylene polymerization and dehydrogenation catalysis [24, 25]. Carrado and his co-workers have studied the decane cracking by using hydroxy-chromium cations in pillared clays as catalysts [26]. Typically the polycations endure dehydration and dehyroxylation during intercalation in clays and impart Brønsted acidity. During hydrolysis the charge of the chromium oligomers can be controlled by the solution chemistry [27]. Partial hydrolysis and polymerization of $Cr(H_2O)_6^{3+}$ can take place rapidly in aqueous solution of pH 2.5–3.5 around 95 °C forming the polycation species such as the dimer $[Cr_2(OH)_2(H_2O)_8]^{4+}$ and trimer $[Cr_3(OH)_4(H_2O)_9]^{5+}$ as given below:

$$Cr(H_2O)_6^{3+} + H_2O \xrightleftharpoons[\leq 100^\circ C]{pH=2.5-3.5} [Cr(H_2O)_5OH]^{2+} + H_3O^+$$

$$2[Cr(H_2O)_5OH]^{2+} \xrightleftharpoons{\text{dimerization}} [Cr_2(H_2O)_8(OH)_2]^{4+} + 2H_2O$$

$$3[Cr(H_2O)_5OH]^{2+} \xrightleftharpoons{\text{polymerization}} [Cr_3(H_2O)_9(OH)_4]^{5+} + 4H_2O + H_3O^+$$

The aqueous equilibria shift rapidly towards the right side with increase in temperature up to 100 °C and OH/Cr ratio higher than unity facilitating the dimerization and polymerization of Cr^{3+} species generating cationic polyoxychromium oligmers of type $[Cr_4(OH)_6(H_2O)_{11}]^{6+}$ and $[Cr_4(OH)_5O(H_2O)_{10}]^{5+}$ [28–30]. Therefore higher loading of uniform chromia clusters on silicate matrix can be achieved by using the polymerized Cr-polycations containing 2–4 metallic atoms than direct loading of metal oxide by impregnating $Cr(H_2O)_6^{3+}$. Polycation method of grafting can also produce defects, and Cr^{3+}, Cr^{6+} and possibly Cr^{5+} surface species on chromia surface.

In general, polycations of metals such as Cr, Al, Zr, V, Ti, and Fe are widely used for pillaring process in various clays and layered materials [28, 30–32]. However the literature suggests that these polycations actively participate in catalytic reactions. Since a vast literature is available on catalytic applications for various impregnated catalysts, using polycations for impregnation is a novel method to generate high acidic species in the mesopores. In this report, first of its kind Cr-polycation sol was grafted on SBA-15 and their molecular interactions with the support were studied. Chromia grafted on SBA-15 by polycation method, and its effect on the structure and reducibility of CrO_x/SBA-15 materials as well as the nature Cr-species grafted on SBA-15 are discussed in detail. The CrO_x/SBA-15 materials have been synthesized by (1) one-pot hydrothermal co-condensation method under highly acidic conditions (pH < 2), (2) Cr-polycation grafting method, and (3) wet impregnation method using $Cr(NO_3)_3$.

2 Experimental

2.1 Synthesis of CrO_x-grafted SBA-15 materials

This section describes the preparation of mesoporous silica SBA-15, Cr-incorporated SBA-15 by direct hydrothermal co-condensation synthesis and by grafting of Cr-polycations. SBA-15 materials were hydrothermally synthesized by following the procedure reported by Zhao et al. [1]

using triblock copolymer P123 ($EO_{20}PO_{70}EO_{20}$) as a template material. Two CrO_x/SBA-15 samples with initial gel composition containing Cr/Si mole ratio of 0.05 and 0.01 were prepared by one-pot synthesis. In this method, Cr species was added simultaneously with tetraethylorthosilicate (TEOS). In a typical synthesis, 4 g of P123 was dissolved in 30 ml of water at room temperature and then 120 mL of 2 M HCl was added under stirring. The required amount of $Cr(NO_3)_3{\cdot}9H_2O$ dissolved in 10 mL of ethanol was added to 8.5 g of TEOS and the mixture was sonicated for 10 min. The Cr-TEOS mixture was then added to the P123 polymer solution under constant stirring at room temperature. The mole composition of the gel for 4 g of P123 was 1:0.017:x:5.6:208 (TEOS:P123:Cr^{3+}, x = 0.05 or 0.01:HCl:H_2O). The resultant solution was stirred for 20 h at 40 °C, followed by aging at 100 °C for 48 h under static conditions. The solid product was filtered, washed with water and ethanol, air dried at 80 °C overnight, and then calcined in nitrogen at 550 °C for 6 h. The calcined samples prepared by one-pot synthesis are denoted as SBA-15-c, Cr/Si(0.01)/SBA-15-c and Cr/Si(0.05)/SBA-15-c.

100 mL of 10 mmol Cr-polycations were prepared in aqueous solution using $Cr(NO_3)_3{\cdot}9H_2O$ as Cr-source and Na_2CO_3 as base [29]. 50 ml 0.2 M $Cr(NO_3)_3{\cdot}9H_2O$ was hydrolyzed by drop wise slowly adding 50 mL of 0.021 M Na_2CO_3 solution while stirring continuously at room temperature (CO_3^{2-}/Cr = 2.1 meq/mmol). Oligomerization of Cr^{3+} has been done by refluxing the mixture at 95 °C for 72 h. The final pH obtained for the Cr-polycation solution was about 3.4 which is similar to the pH values reported [20, 33]. The cooled Cr-polycation solution was grafted on 1 g of SBA-15 (10 mmol of Cr/g) by impregnation method. In this method, 1 g of SBA-15 was dispersed in 100 ml of cooled Cr-polycation solution whilst constant stirring for 6 h at room temperature. The mixture was dried in oven at 80 °C until the solvent was completely evaporated. The dried product was washed thoroughly with distilled water until nitrate free, then dried in oven at 80 °C and finally calcined in air at 400 °C for 3 h. This calcined sample is denoted as CrO_x-poly/SBA-15-c.

Similarly, 20 wt% CrO_x/SBA-15 material was prepared by wet impregnation method using $Cr(NO_3)_3{\cdot}9H_2O$. The required amount of metal precursor was dissolved in 20 ml of H_2O and the solution was added slowly to 1 g of SBA-15 powder. The slurry formed by the addition of $Cr(NO_3)_3$ solution to SBA-15 was stirred continuously for 6 h at room temperature. It was then dried in oven at 80 °C to evaporate H_2O completely. The dried product was calcined in air at 400 °C for 3 h. The calcined sample is denoted as CrO_x-imp/SBA-15-c. For comparison, $Cr(OH)_3$ was prepared by precipitating 0.1 M $Cr(NO_3)_3{\cdot}9H_2O$ with 5 M NaOH at pH = 10. Further the chromium hydroxide was calcined in air at 400 °C for 3 h to obtain green Cr_2O_3. All the above uncalcined samples are denoted as SBA-15-uc, Cr/Si(0.01)/SBA-15-uc, Cr/Si(0.05)/SBA-15-uc, CrO_x-poly/SBA-15-uc and CrO_x-imp/SBA-15-uc.

2.2 Characterization

The powder samples were characterized by low angle X-ray powder diffraction (XRD). The XRD pattern were recorded in the low angle region ($2\theta = 0.5°$–$3°$) and wide angle region ($2\theta = 10°$–$80°$) using a Bruker D8Advance X-ray diffractometer employing nickel filtered CuK_α radiation (1.5418 Å) at a scan rate of $0.1°\ s^{-1}$. The surface areas of the samples were measured using Brunauer–Emmett–Telleller (BET) method by N_2 adsorption and desorption at 77 K in a Micromeritics ASAP2000 system. The samples were pretreated by degassing at 473 K under vacuum for 12 h. The mean pore diameter and pore size distribution were determined from the desorption branch of the isotherm using Barrett–Joyner–Halenda (BJH) method. The specific surface area was calculated by (BET) model. The micropore surface area and micropore volume are obtained by t-plot using Harkins and Jura (HJ) method.

Diffuse reflectance UV–Vis spectra were collected from 200 to 700 nm on a JASCO V-570 spectrophotometer equipped with an integrating sphere. A halon white reflectance standard was used as a reference material. 1.0 cm path length quartz cuvettes were used for analyzing solutions. The sample morphology of the silicate samples was studied by both scanning and transmission electron microscopy (FEI Quanta 200 and JEOL 3010 HRTEM). SEM and TEM micrographs were obtained from the powder samples dispersed on carbon tape and carbon-coated copper grids, respectively.

NH_3-TPD and H_2-TPR experiments were carried out on Micromeritics Chemisorb 2750 apparatus using TCD detector and a fixed-bed flow micro-reactor in the temperature range of 25–750 °C. The temperature of the reactor was measured by a K-type thermocouple located in a quartz capillary immersed in the sample bed. Before conducting the NH_3-TPD experiment, 100 mg of each calcined sample was outgassed at 500 °C for 1 h in 20 mL/min He flow, and cooled to room temperature and saturated in a flow of 4.5 vol% NH_3 in He (20 mL/min) for 30 min. The sample was then purged in He flow for about 35 min until a constant baseline level was attained. NH_3-desorption experiment was carried out by raising the temperature linearly at the rate of 10 °C/min in 20 mL/min He flow. For H_2-TPR experiments, 100 mg of each calcined sample was degassed at 500 °C for 1 h in 20 mL/min oxygen flow. The sample was cooled to room temperature and the H_2-TPR experiment was carried out in a flow of H_2 gas (5% H_2 in Ar, 20 mL/min) at a heating rate of 20 °C/min

up to 750 °C. A gas condenser trap at −80 °C is placed prior to the TCD to remove water.

The thermogravimetric analysis (TGA) was done on Q-500 Quantachrome (TA-Instruments) in the range of 40–800 °C. Fourier transform infrared (FTIR) spectra were recorded on a Shimadzu FTIR-8100 spectrophotometer using thin wafer containing 1% of sample in KBr. X-ray photoelectron spectroscopy (XPS) measurements were performed on Omicron Nanotechnology spectrometer with MgKα monochromatic source operating at 15 kV and 20 mA. The spectra were recorded using 100 eV analyzer pass energy and corrected with respect to C1s at 285 eV. The ^{29}Si MAS NMR spectra of SBA-15 and CrO_x grafted SBA-15 materials prepared by one-pot method were recorded using Bruker Avance 400 spectrometer at resonance frequency of 79.49 MHz for ^{29}Si nuclei. All the chemical shifts are reported in ppm (δ) relative to external tetramethylsilane (TMS). The ^{29}Si MAS NMR spectra were recorded with a sample spinning rate of 8 kHz.

3 Results and discussion

3.1 Structure of CrO_x-SBA-15 samples

The low angle XRD patterns of both SBA-15 and Cr-modified SBA-15 calcined samples are shown in Fig. 1. The samples show characteristic intense peak around $2\theta = 1.0°$ corresponding to (100) reflection followed by two weaker peaks related to (110) and (200) reflections, typical of a hexagonal lattice with p6 mm symmetry of SBA-15. In general, isomorphic substitution is done with the species having similar ionic radius of Si^{4+} (0.40 Å) with tetrahedral geometry. Cr^{3+} ion (0.62 Å) is larger than Si^{4+} and prefers octahedral coordination as in Cr_2O_3, and it is hard to incorporate in silica framework. However, Cr^{6+} (0.44 Å) with tetrahedral geometry can be substituted in silica framework resulting in increased lattice parameter of SBA-15. But the efficiency of isomorphic incorporation of metal ions into the silica framework by direct-synthesis is always low because of the dissolution of metal ions into the solution at very low pH (< 2). Under these conditions the corresponding hydrolysis and condensation rates of metal ions differ with respect to Si^{4+}. Therefore the increment in the unit cell constants is trivial in Cr/Si(0.01)/SBA-15-c and Cr/Si(0.05)/SBA-15-c (99 and 98 Å respectively) samples as compared to SBA-15-c (97 Å). However, well resolved intense peaks indicate that both Cr/Si(0.01)/SBA-15-c and Cr/Si(0.05)/SBA-15-c samples clearly maintain the same structural symmetry of SBA-15 matrix. The lattice parameters for all the samples are determined by the equation $a_o = 2d/\sqrt{3}$ for a primitive hexagonal lattice, where d is the inter-planar distance of (100) plane. The textural parameters

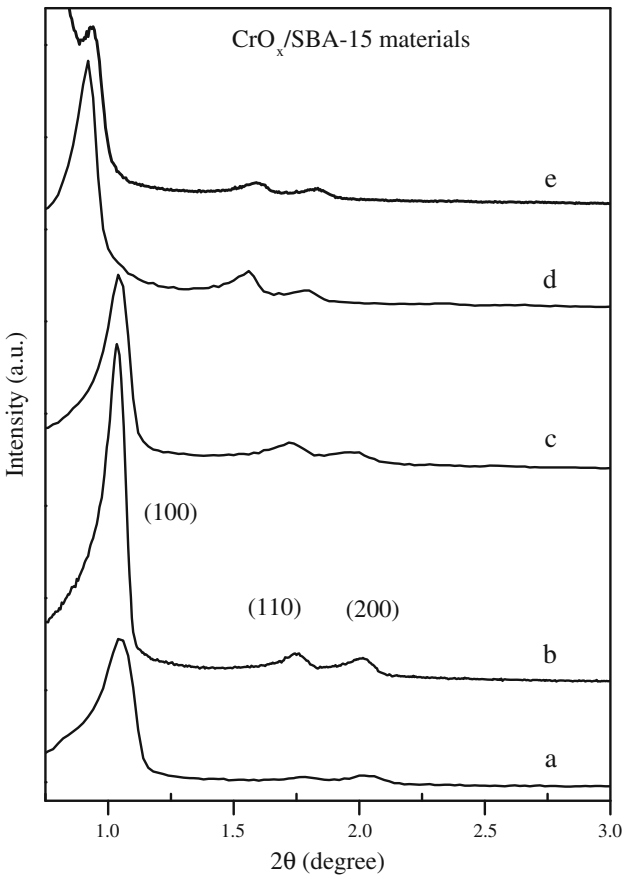

Fig. 1 Low angle XRD patterns of SBA-15 and Cr-modified SBA-15 calcined samples: *a* SBA-15-c, *b* Cr/Si(0.01)/SBA-15-c, *c* Cr/Si(0.05)/SBA-15-c, *d* CrO_x-imp/SBA-15-c, *e* CrO_x-poly/SBA-15-c

deduced by XRD and BET isotherms are given in Table 1. Both the impregnated samples, CrO_x-imp/SBA-15-c and CrO_x-poly/SBA-15-c, also exhibit characteristic pattern of SBA-15, and chromia loading do not affect the frame work of SBA-15. However, the polycation grafted sample, CrO_x-poly/SBA-15-c, seems to have higher wall thickness compared to other samples. This is due to the anchoring of polycations and their transformation to uniform chromia coating on SBA walls by calcination. The wide angle XRD patterns of Cr-modified calcined SBA-15 samples are shown in the Fig. 2. The XRD pattern of α-Cr_2O_3 sample is also included for comparison. The diffraction peaks of chromia crystallites in CrO_x-imp/SBA-15-c and CrO_x-poly/SBA-15-c samples match with reflections at 24.5°, 33.6°, 36.2°, 41.6°, 50.3°, 54.9°, 63.5° and 65.2° of bulk rhombohedral phase of α-Cr_2O_3 (JCPDS No.: 84-1616). This confirms the formation of α-Cr_2O_3 crystallites in SBA-15 matrix in both the impregnated samples. The CrO_x crystallite sizes in CrO_x-imp/SBA-15-c and CrO_x-poly/SBA-15-c samples are about 4.2 and 10.5 Å, respectively. The crystallite size is larger when Cr-polycation source is used in the impregnation, as expected. However, there is no XRD evidence of

Table 1 Textural properties of the calcined SBA-15 and Cr-modified SBA-15 materials synthesized by one-pot and impregnation methods

Sample	Planar distance ($d_{(100)}$) (Å)	Lattice constant (a_o) (Å)[a]	Wall thickness ($a_o - D$) (Å)[b]	Pore diameter (D) (Å)[c]	Surface area (BET) m^2/g	Micro pore area (m^2/g)[d]	Total pore volume (cm^3/g)[e]	Micro pore volume (cm^3/g)[d]
SBA-15-c	84	97	45	52	664	221	0.68	0.103
Cr/Si(0.01)/SBA-15-c	86	99	47	52	831	101	0.93	0.041
Cr/Si(0.05)/SBA-15-c	85	98	40	58	983	226	1.09	0.098
CrO_x-imp/SBA-15-c	96	111	47	64	326	58	0.85	0.026
CrO_x-poly/SBA-15-c	95	109	51	58	385	60	0.80	0.027

[a] a_o was calculated by using the equation $a_o = 2d/\sqrt{3}$

[b] Wall thickness = a_o − pore diameter (D)

[c] The peak maximum of pore size distribution calculated from the N_2 desorption branch using the BJH method

[d] t-plot using Harkins and Jura method

[e] The total pore volume estimated from the amounts adsorbed at a relative pressure (P/P_o) of 0.99

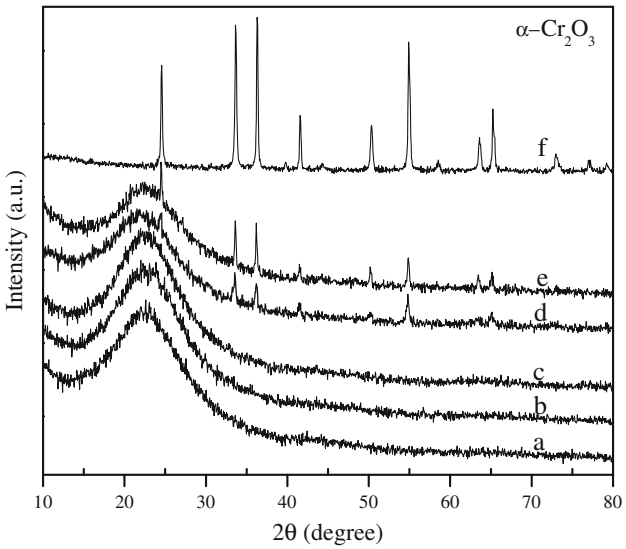

Fig. 2 Wide angle XRD patterns of SBA-15 and Cr-modified SBA-15 calcined samples: *a* SBA-15-c, *b* Cr/Si(0.01)/SBA-15-c, *c* Cr/Si(0.05)/SBA-15-c, *d* CrO_x-imp/SBA-15-c, *e* CrO_x-poly/SBA-15-c, *f* α-Cr_2O_3

α-Cr_2O_3 crystallites existing in Cr/Si(0.01)/SBA-15-c and Cr/Si(0.05)/SBA-15-c samples prepared by one-pot synthesis. In these cases chromia does not form crystallites but spread out in amorphous form on SBA-15 matrix. There is a clear difference in chromia dispersion which is affected by the polycation sol or aqueous Cr-source (polycation and nitrate) and used and preparative method employed.

3.2 SEM and TEM studies

The electron micrographs of calcined SBA-15 and Cr-modified SBA-15 prepared by co-condensation (one-pot) methods are shown in Fig. 3. SEM images of SBA-15-c depict the typical rod like hexagonal morphology of few microns length Fig. 3A1, A2. The sample Cr/Si(0.01)/SBA-15-c, however, shows two different morphologies. One is of agglomerated spheres Fig. 3B1, B2 and the other is normal 2D-hexagonal rod-like morphology Fig. 3B3, B4, similar to pure SBA-15. The factors such as pH, electrolyte and aging temperature can affect the interaction between the surfactant micelles and the inorganic silica precursor through $(S^0H^+)(X^-I^+)$ mechanism which decides the final structure of mesoporous materials during the self-assembly process [1, 34, 35]. At pH < 2 and low concentration of Cr^{3+} ions, the metal ions can interact with ethoxy groups of the nonionic surfactant and facilitate partial formation of spherical silica particles due to reduced interactions between the silica source and surfactant leading to incomplete condensation. However, at higher concentration of Cr^{3+} ions, Cr/Si(0.05)/SBA-15-c material shows only rod-like hexagonal morphology (Fig. 3C1,C2).

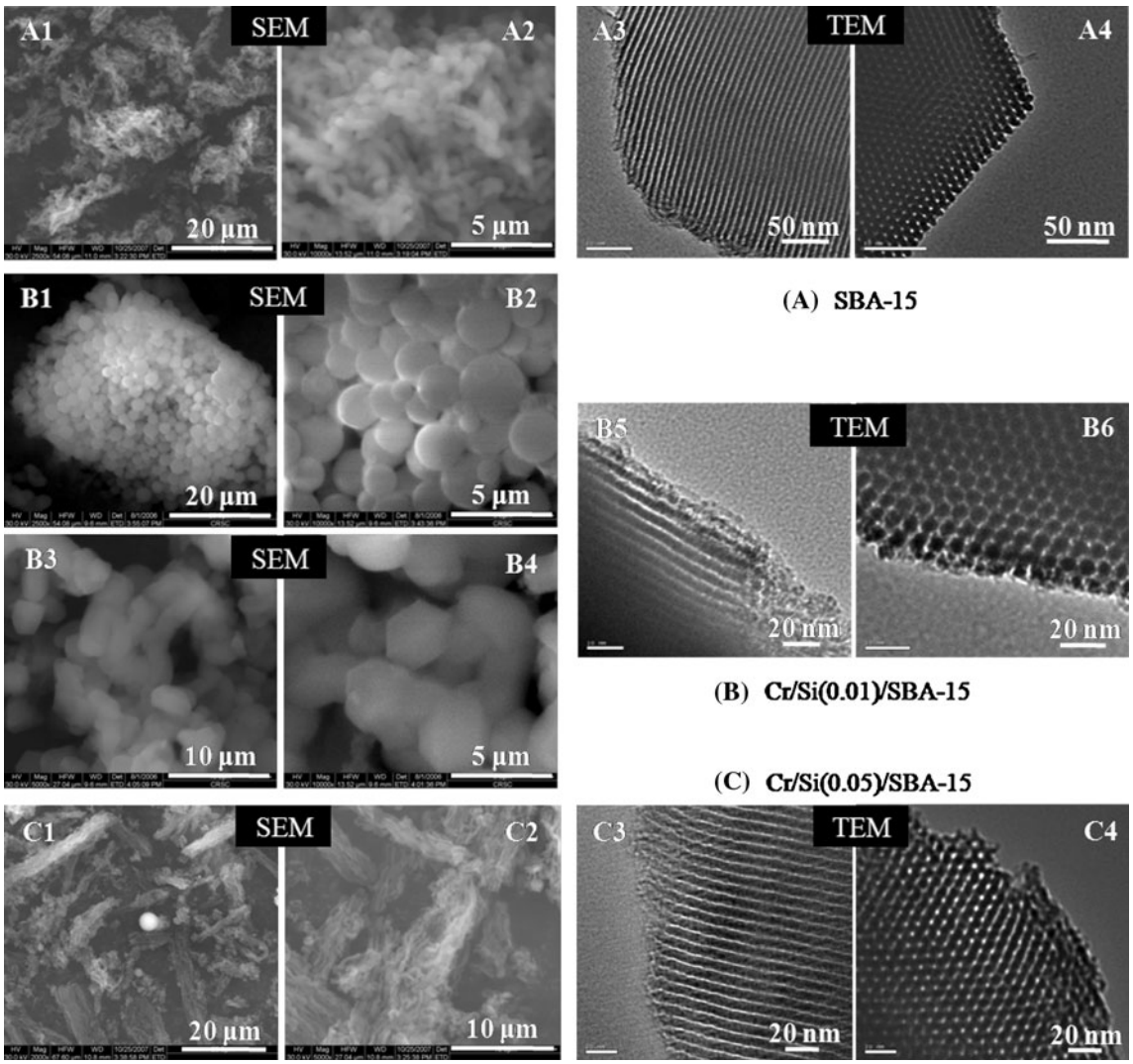

Fig. 3 SEM and TEM micrographs of calcined SBA-15 and Cr-modified SBA-15 samples prepared by one-pot synthesis: (*A1–A4*) SBA-15-c, (*B1–B6*) Cr/Si(0.01)/SBA-15-c, (*C1–C4*) Cr/Si(0.05)/SBA-15-c

The transmission electron microscopic images clearly reveal uniform channels of pores with long range ordered arrays for all the SBA-15 materials. They show parallel directions in Fig. 3A3, B5, C3 and perpendicular directions in Fig. 3A4, B6, C4 characteristic to SBA-15 pore system having long range ordered 2D pores with honey comb structure. These images confirm the structural features of the SBA-15 silicate matrix and there is no evidence for the agglomerated chromia particles in the pores. This suggests that chromia is finely dispersed in the porous structure of SBA-15.

3.3 Thermo gravimetric analysis

The weight loss pattern of uncalcined samples, SBA-15-uc, Cr/Si(0.01)/SBA-15-uc, Cr/Si(0.05)/SBA-15-uc, CrO_x-imp/SBA-15-uc and CrO_x-poly/SBA-15-uc, have been studied by thermogravimetry. The TG curves of uncalcined SBA-15 and Cr-modified SBA-15 materials are shown in the Fig. 4. The one-pot synthesized samples SBA-15-uc, Cr/Si(0.01)/SBA-15-uc and Cr/Si(0.05)/SBA-15-uc exhibit similar loss patterns which are typical of SBA-15 [1]. The initial weight loss of about 12% in all these samples below 200 °C is due to desorption of condensed water. Decomposition of surfactant molecules in these samples is observed above 200 °C. As synthesized SBA-15 materials are known to show different weight losses above 200 °C depending on the washing methods employed using water and ethanol alternately. The surfactant removal is not uniform during the washing procedures and often reflected in TGA [36].

Both the impregnated samples, CrO_x-imp/SBA-15-uc and CrO_x-poly/SBA-15-uc, however, show sharp and considerable initial weight loss below 100 °C due to the desorption of large amount of physisorbed condensed water

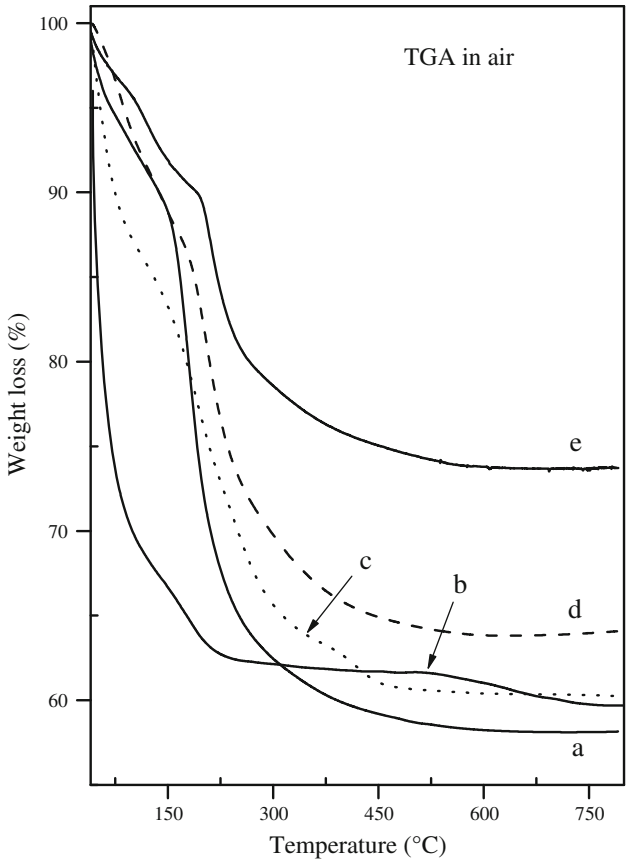

Fig. 4 TG analysis of SBA-15 and Cr-modified SBA-15 uncalcined samples in air atmosphere: *a* Cr/Si(0.05)/SBA-15-uc, *b* CrO_x-imp/SBA-15-uc, *c* CrO_x-poly/SBA-15-uc, *d* SBA-15-uc, *e* Cr/Si(0.01)/SBA-15-uc

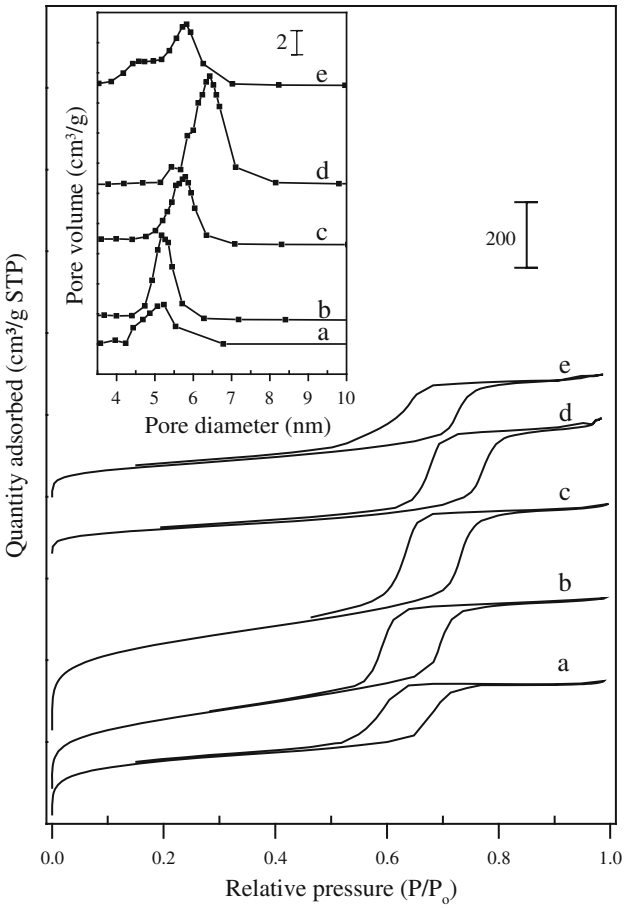

Fig. 5 N_2 adsorption–desorption isotherms at 77 K of SBA-15 and Cr-modified SBA-15 calcined samples: *a* SBA-15-c, *b* Cr/Si(0.01)/SBA-15-c, *c* Cr/Si(0.05)/SBA-15-c, *d* CrOx-imp/SBA-15-c, *e* CrOx-poly/SBA-15-c (*inset* shows the pore size distribution of the corresponding samples)

in the pores. The saturation of second weight loss for CrO_x-imp/SBA-15-uc is due to nitrate decomposition around 400 °C followed by a weight loss of about 2% between 520 and 750 °C signifies complete conversion to α-Cr_2O_3 phase. In the case of CrO_x-poly/SBA-15-uc sample, the Cr-polycation species is converted to α-Cr_2O_3 phase by losing the coordinated water between 100 and 500 °C.

3.4 Textural analysis

Figure 5 displays the nitrogen adsorption–desorption isotherms of all chromia containing calcined SBA-15 samples viz., Cr/Si(0.01)/SBA-15-c and Cr/Si(0.05)/SBA-15-c, CrO_x-imp/SBA-15-c, CrO_x-poly/SBA-15-c compared to calcined SBA-15-c sample. The N_2 adsorption–desorption isotherms obtained are of type IV according to the IUPAC classification and exhibited a H1-type broad hysteresis loop, which is typical of large-pore mesoporous solids. Isotherms exhibited a sharp increase at capillary condensation steps at relative pressure range between 0.50 and 0.80, indicating the presence of uniform mesopores (52–64 nm). The inset in Fig. 5 shows the mesoporous materials having the mean pore diameters ranging from 5.1 to 6.4 nm obtained from the desorption branches of isotherms using BJH method. The narrow pore size distribution implies uniform pores for materials synthesized by one-pot method (b and c in Fig. 5). The BET specific surface areas obtained for calcined samples of SBA-15-c, Cr/Si(0.01)/SBA-15-c and Cr/Si(0.05)/SBA-15-c are 664, 831 and 983 m^2/g respectively (Table 1). The increase in surface area and total pore volume with increased Cr content indicate considerable influence of chromium ions in one-pot synthesis method where Cr ions seem to facilitate the condensation of silicate groups forming extended silica frameworks.

Considerable decrease in total BET surface area for CrO_x-imp/SBA-15-c and CrO_x-poly/SBA-15-c materials elucidate the grafting of chromium oxide crystallites in SBA-15 pores (Table 1). Diminution of micropore area and volume of these materials demonstrate the inclusion of chromium oxide crystallites into the pores of SBA-15. The

loading is exhibited by a broad shoulder towards the lower pore diameter for both CrO_x-imp/SBA-15-c and CrO_x-poly/SBA-15-c materials.

3.5 UV–DRS study

DR UV–vis spectroscopy has been a very useful tool to identify the chemical environment and coordination states of chromium ions [20]. In general the oxidation states of chromium vary from +2 to +6. Typically Cr^{3+} (d^3) and Cr^{6+} (d^0) ions are stable with octahedral and tetrahedral symmetries respectively. In acid solution, Cr^{3+} ions exhibit octahedral symmetry and hydrolyze with increase in pH. The tetrahedral coordinated Cr^{6+} ions exist as polyoxoanions at very low pH such as chromate (CrO_4^{2-}), dichromate ($Cr_2O_7^{2-}$), trichromate ($Cr_3O_{10}^{2-}$) and polychromates. The charge-transfer and d–d transitions of Cr can be probed using DRS spectroscopy in the range 200–800 nm (50,000–12,500 cm^{-1}) which is useful to diagnose Cr^{6+} in tetrahedral and Cr^{3+} in octahedral symmetry. Both these transitions are characteristic to the oxidation state of Cr and the geometry of Cr ions in the coordination sphere of oxygen ions, in chromia clusters. The LM charge-transfer transitions are of the type $O^{2-} \rightarrow Cr^{6+}$ which are typical for Cr^{6+} ions in chromate and dichromate ions. Cr^{3+} ions show characteristic d–d transitions which are weaker than the charge transfer transitions. All the transitions exhibited by SBA-15 and Cr-modified samples prepared by both one-pot and impregnation methods are summarized in the Table 2. Fig. 6 shows two typical characteristic d–d transitions for Cr^{3+} at 409 nm ($^4A_{2g} \rightarrow {}^4T_{1g}$), 575 nm ($^4A_{2g} \rightarrow {}^4T_{2g}$) and an additional band at 296 nm when $Cr(NO_3)_3 \cdot 9H_2O$ dissolved in water is blue in colour. When Cr^{3+} is polymerized, the 296 nm band has disappeared and the d–d transitions red-shifted to 419 and 580 nm respectively. These changes indicate that the green colour Cr-polycation solution contains Cr^{3+} oligomers essentially in the form of dimers [33].

Figure 7 displays the UV–vis spectra of calcined and as-synthesized SBA-15, Cr/Si(0.01)/SBA-15 and Cr/Si(0.05)/SBA-15 materials. All these three samples are white in colour. Both calcined Cr-SBA-15 materials exhibit electron excitations from the ligand orbitals into the empty $e_g\left(d_{z^2}, d_{x^2-y^2}\right)$ and $t_{2g}(d_{xy}, d_{xz}, d_{yz})$ orbitals of Cr^{6+} with a broad band around 348 nm and a weak shoulder around 454 nm [37]. The weak shoulder at higher wavelength ($\sim$450 nm) indicates the presence of dichromate species and the broad band 320–390 nm is due to mono-chromate species [20, 38–40]. At pH < 2, polymerized chromium oxide species are favourable and the polymerization seems to be restricted to dichromate formation inside the pores. The uncalcined SBA-15-uc shows very intense band at 211 nm which lost intensity after the calcination. Three clear DRS bands are seen at 211, 250 and 292 nm for calcined SBA-15. These bands are attributed to $O \rightarrow Si^{4+}$ charge transfer transitions related to SBA framework with different condensations of SBA-15 and Cr-SBA-15 samples.

The UV–Vis DR spectra for the impregnated uncalcined and calcined samples of CrO_x-imp/SBA-15 and CrO_x-poly/SBA-15 in comparison to $Cr(OH)_3$ and Cr_2O_3 are shown in the Fig. 8. Both calcined and uncalcined impregnated samples are light-green in colour. The uncalcined CrO_x-imp/SBA-15 and CrO_x-poly/SBA-15 samples display DRS bands at 298 nm, 420 nm, 594 nm characteristic of octahedral coordinated Cr^{3+} ions in solid similar to that of $Cr(OH)_3$. Upon calcination these samples show DRS bands at 266, 295, 344, 370, 459, 470 and 605 nm and the spectral features show subtle differences in nitrate (Fig. 8d) and polycation (Fig. 8e) impregnated samples. Both the samples show transitions related to Cr^{3+} and Cr^{6+} ions

Table 2 UV–Vis DR spectra of SBA-15 and Cr-modified SBA-15 materials synthesized by one-pot and impregnation methods; UV-Vis spectral transitions of aqueous solutions of $Cr(NO_3)_3$ and Cr-polycation sol are given in the last two rows

Sample	Uncalcined samples			Calcined samples		
	SBA frame work (nm)	d–d transitions (nm)		SBA frame work (nm)	CT-1 (nm)	CT-2 (nm)
		$^4A_{2g} \rightarrow {}^1T_{2g}$	$^4A_{2g} \rightarrow {}^1T_{2g}$			
SBA-15	210, 262, 293	–	–	213, 250, 292	–	–
Cr/Si(0.01)/SBA-15	210, 262, 293	–	–	211, 250, 293	348	454
Cr/Si(0.05)/SBA-15	210, 262, 293	–	–	211, 250, 293	348	454
CrO_x-imp/SBA-15	210, 262, 295	421	582	211, 250, 292	352	467
CrO_x-poly/SBA-15	210, 295	421	593	211, 250, 292	356	468, 605
$Cr(OH)_3$	–	421	593	–	–	–
Cr_2O_3	–	–	–	–	356, 468	605
$Cr(NO_3)_3$ solution	–	409	575	–	296	–
Cr-polycation sol	–	419	580	–	–	–

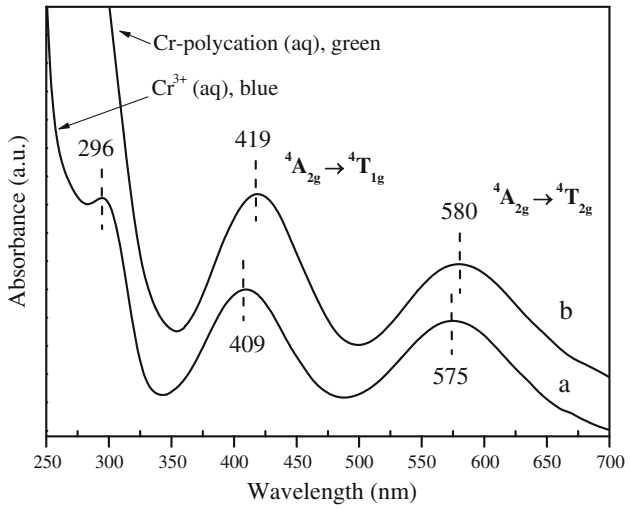

Fig. 6 UV-Vis spectra of aqueous solutions of *a* blue $Cr(NO_3)_3 \cdot 9H_2O$ and *b* green Cr-polycation sol

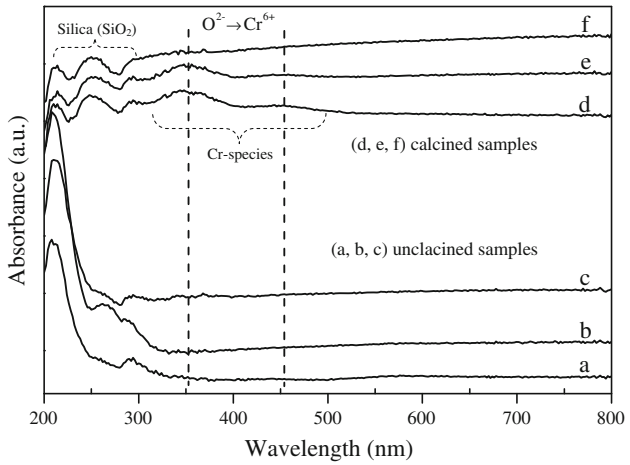

Fig. 7 UV-Vis DR spectra of SBA-15 and Cr-modified SBA-15 samples prepared by one-pot method: *a* Cr/Si(0.05)/SBA-15-uc, *b* Cr/Si(0.01)/SBA-15-uc, *c* SBA-15-uc, *d* Cr/Si(0.05)/SBA-15-c, *e* Cr/Si(0.01)/SBA-15-c, *f* SBA-15-c

present on the surfaces. The polycation sample shows additional band at 605 nm due to the octahedrally coordinated Cr^{3+} in Cr_2O_3 clusters. This implies that upon calcination the nitrate and polycation precursors give rise to different chromia species for which the Cr^{3+}/Cr^{6+} ratios vary. The red shift in the DRS bands observed in calcined samples (Fig. 8a–c) with respect to uncalcined samples (Fig. 8d–f) has originated from the pseudo-ocatahedral symmetry of Cr^{3+} ion in the solid state [41].

3.6 ^{29}Si MAS-NMR study of CrO_x-SBA-15 samples prepared by one-pot method

The extent of silica condensation in the presence of Cr is studied by ^{29}Si MAS NMR. The degree of condensation in

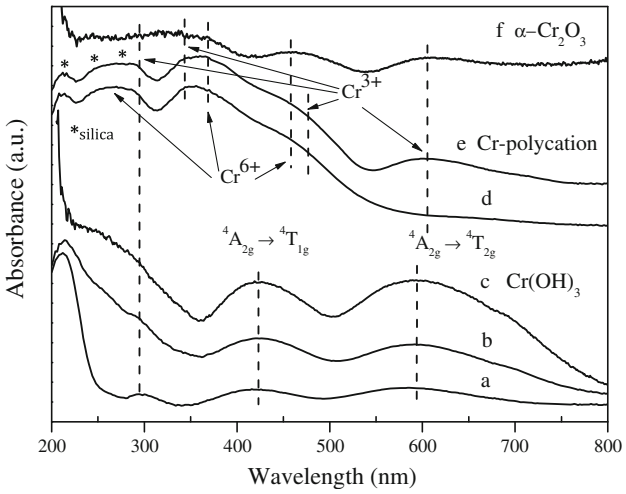

Fig. 8 UV-Vis DR spectra of CrO_x and Cr-modified SBA-15 samples prepared by impregnation method: *a* CrO_x-imp/SBA-15-uc, *b* CrO_x-poly/SBA-15-uc, *c* $Cr(OH)_3$, *d* CrO_x-imp/SBA-15-c, *e* CrO_x-poly/SBA-15-c, *f* Cr_2O_3

SBA materials has been investigated by ^{29}Si chemical shifts in the range of −60 to −120 ppm in which a variety of silicate species, $Q^n = Si(OSi)_n(OH)_{4-n}$, n = 0–4, are identified in the final products [42]. Figure 9 shows ^{29}Si MAS NMR spectra of calcined SBA-15-c, Cr/Si(0.01)/SBA-15-c and Cr/Si(0.05)/SBA-15-c samples. SBA-15-c sample shows broad ^{29}Si feature in Fig. 9a with three different degrees of condensation at −88 ppm (Q^2), −100 ppm (Q^3) and −105 ppm (Q^4) [1, 42]. The broad peaks indicate local disorder present in the silica framework. However, unlike in SBA-15-c sample, chromia modified SBA-15 materials show well resolved peaks Fig. 9b and c. Addition of chromium precursor to the initial silica gel resulted in highly dense condensed silica product which shows no Q^2 peak. This shows that there is high degree of condensation in the presence of chromium which can decrease the number of geminal silanol, Si-$(OH)_2$, groups in SBA-15 walls. The Q^3 and Q^4 peaks became sharper and shifted to upfields, respectively, at −104 and −114 ppm for Cr/Si(0.01)/SBA-15-c and Cr/Si(0.05)/SBA-15-c samples. This can happen in the confined electronic environment at the interface of CrO_x anchored to silica matrix of SBA-15 [42]. Hence an increased upfield shift with increase in the amount of chromium precursor loading signifies more CrO_x grafted over silanol groups of SBA-15, which is consistent with the UV–Vis DRS study.

3.7 XPS O1s region of SBA-15 materials

The O1s lines of materials such as SiO_2 and Al_2O_3 are known to produce broad energy loss features in XPS. The SBA-15 materials are studied for the occurrence of such features which may show some differences in Cr-grafted on

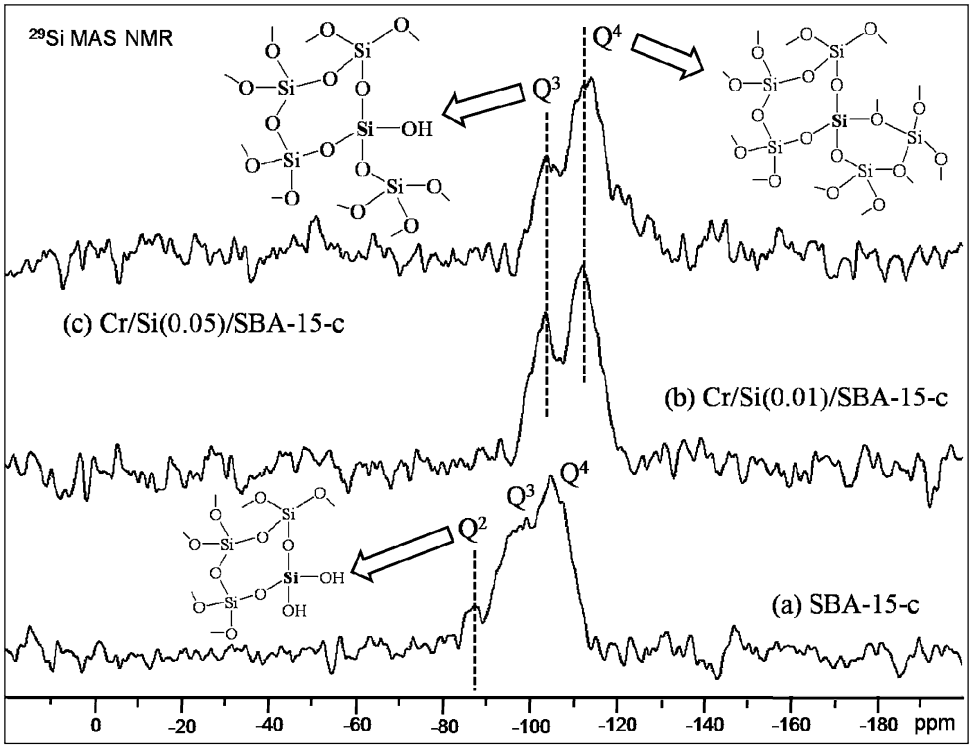

Fig. 9 ^{29}Si-MAS NMR spectra of Cr-modified SBA-15 calcined samples prepared by one-pot method: *a* SBA-15-c, *b* Cr-SBA-15(0.01)-c, *c* Cr-SBA-15(0.05)-c

surfaces of SBA-15. Figure 10 shows the O1s spectra of Cr-SBA-15 samples. All the samples display broad humps at around 22 eV from the intense main O1s peaks at 532.8–533.5 eV. The high energy broad features occur because of the energy loss due to the interaction of O1s photoelectrons with the electrons in the surface region of the SBA walls. The main O1s peaks around 533 eV also corroborates the presence of sub-monolayers of surface chromia chemically bonded to silanol groups [5]. This study however shows that there is no significant effect of surface CrO_x grafting on the energy loss peaks.

3.8 H_2-TPR study

The redox mechanism in chemical transformations depends upon the ease of the reducibility of oxide particles. Chromia samples show complex reduction profiles and there are discrepancies in H_2-TPRs of chromia in the literature [5, 43]. The reduction profiles of chromia depend on parameters such as method of preparation, calcination temperature, support material, nature of interaction of chromia with supports and the type of chromium species (i.e. isolated CrO_3, CrO_4^{2-}, $Cr_2O_7^{2-}$, polychromates and crystalline α-Cr_2O_3) grafted on the surface. The relative stability of Cr-species in different oxidation states strongly depends on the nature of interaction between chromia and SBA-15 through the surface silanol groups. The redox nature of the chromia present in Cr-SBA-15 samples has been studied by H_2-TPR and the profiles of the calcined samples are displayed in Fig. 11. No reduction band is detected for the SBA-15 support. It is reasonably established from earlier studies that $Cr^{6+} \rightarrow Cr^{3+}$ and $Cr^{3+} \rightarrow Cr^{2+}$ reductions occur below and above 410 °C respectively [43]. These reduction regions are clearly distinguished in our study but profiles are very different. The one-pot synthesized samples show small $Cr^{6+} \rightarrow Cr^{3+}$ reduction profiles at 300–375 °C due to surface chromium species (Fig. 11b, c). The impregnated samples show intense TPR profiles between 300 and 520 °C indicating the reduction of both Cr^{6+} and Cr^{3+} ions. It appears that the Cr^{6+}/Cr^{3+} ratio is higher in polycation impregnated sample than the nitrate impregnated sample. By comparing the DRS and TPR results it is concluded that Cr^{6+} is present in all the calcined samples while Cr^{3+} species occurs predominantly in the impregnated samples.

3.9 FTIR study

Like SiO_2, SBA-15 has a covalent framework which can be severely hydroxylated. It can predominantly stabilize Brønsted acidic groups such as isolated (single), $(O)_3$-Si–OH and geminal $(O)_2$-Si–$(OH)_2$ silanol groups on its surface. The presence of these groups is indicated in the ^{29}Si MAS NMR spectra (Fig. 9). These surface silanol groups are important for grafting chromia species on SBA-15. Further in IR study, calcined SBA-15 and Cr-modified SBA-15 samples show various silicate framework vibrations in the region 400–1,300 cm^{-1} with Si–O–Si bending modes around 465 cm^{-1}, Si–O–Si symmetric stretch at 806 cm^{-1}

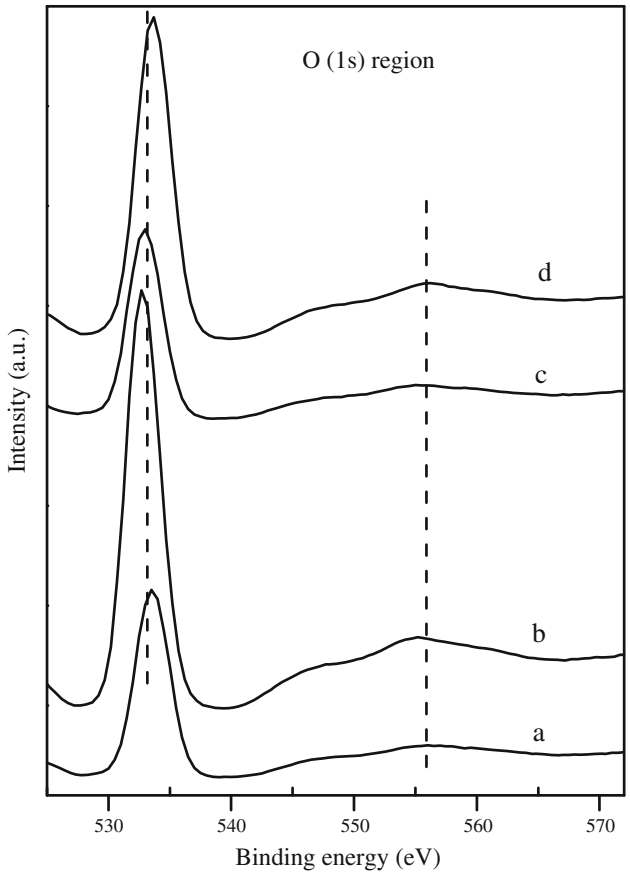

Fig. 10 XPS O1s region of Cr-modified SBA-15 calcined samples: *a* Cr/Si(0.01)/SBA-15-c, *b* Cr/Si(0.05)/SBA-15-c, *c* CrO_x-imp/SBA-15-c, *d* CrO_x-poly/SBA-15-c

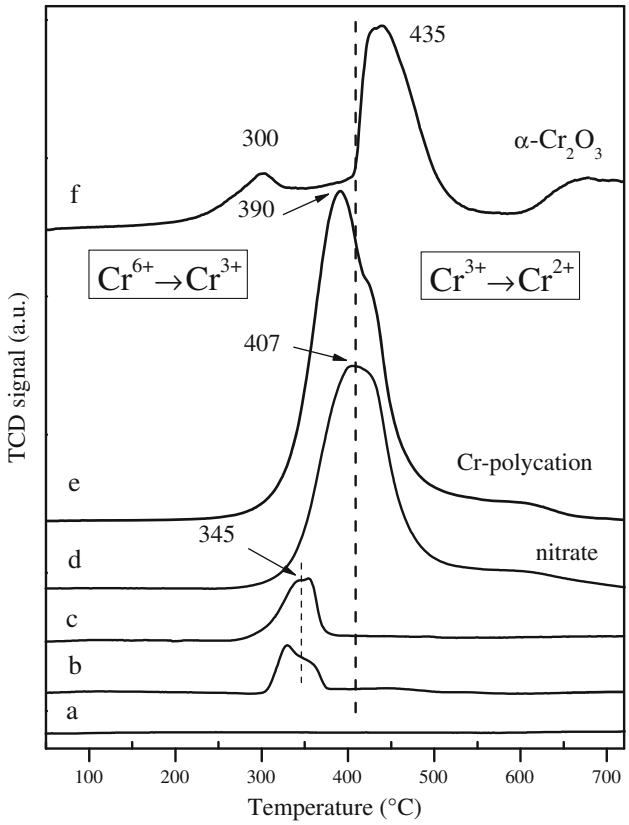

Fig. 11 H_2 reduction profiles of SBA-15 and Cr-modified SBA-15 calcined samples: *a* SBA-15-c, *b* Cr/Si(0.01)/SBA-15-c, *c* Cr/Si(0.05)/SBA-15-c, *d* CrO_x-imp/SBA-15-c, *e* CrO_x-poly/SBA-15-c, *f* α-Cr_2O_3

and Si–O–Si asymmetric stretch around 1,083 cm^{-1} [7, 11]. A broad envelope around 3,450 cm^{-1} is bonded O–H stretching vibrations of adsorbed water as well as surface and bridged hydroxyl groups (full spectra not shown). Similarly the vibrational band at 1,635 cm^{-1} represents the H–O–H bending vibrations (δ_{H-O-H}) of free water molecules attached to SBA-15 [7, 32]. Figure 12 shows the IR spectral regions at 500–700 and 1,400–1,700 cm^{-1}. These spectra distinguish the –OH groups associated with SBA-15 and hydrated CrO_x species. The bands at 573 and $\sim$ 620 cm^{-1} are due to extra framework hydrated CrO_x species present on the pore surfaces which are rarely reported in the literature [44]. However, Cr-polycation impregnated sample shows uniquely intense band at 573 cm^{-1} compared to all other samples. The bending region (δ_{H-O-H}) also distinguishes the hydroxyl groups associated with SBA-15 framework and chromia species (Fig. 12). In the case of one-pot synthesized samples, chromia is present on SBA-15 in the form of isolated and dehydrated CrO_x species in the submonolayer regime, while in the impregnated samples, chromia is grafted as hydrated α-Cr_2O_3 crystallites [45]. The molecular nature of various chromia species is shown in Fig. 13.

3.10 Temperature programmed desorption (NH_3-TPD)

The adsorption of NH_3 on SBA-15 can occur through hydrogen bonding with the oxygen of silanol group or through hydrogen bond between the nitrogen atom and the hydrogen of silanol group. Therefore, the silanol groups are responsible for mild Brønsted acidity. Ammonia desorption from SBA-15 is reported to occur below 150 °C depending on the experimental conditions [3, 4, 46]. Figure 14 illustrates the NH_3 desorption beahviour of various SBA-15 samples which show strong NH_3 desorption below 150 °C. The desorption peak at 90 °C is attributed to physisorbed NH_3 attached to the weak acidic sites on SBA-15 by hydrogen bonding. However, there is almost no NH_3 desorption observed above this temperature due to the fact that SBA-15 does not possess strong acid sites. There are weak NH_3 desorption features observed in the range of 200–700 °C by CrO_x/SBA-15 samples shown in the inset of Fig. 14. The amount of NH_3 desorbed above 200 °C is insignificant compared to the desorption peaks at 90 °C. Though weak, there two broad desorption regions that can be identified at 250–450 °C and above 450 °C (inset of Fig. 14). The first one is due to NH_3 desorption from

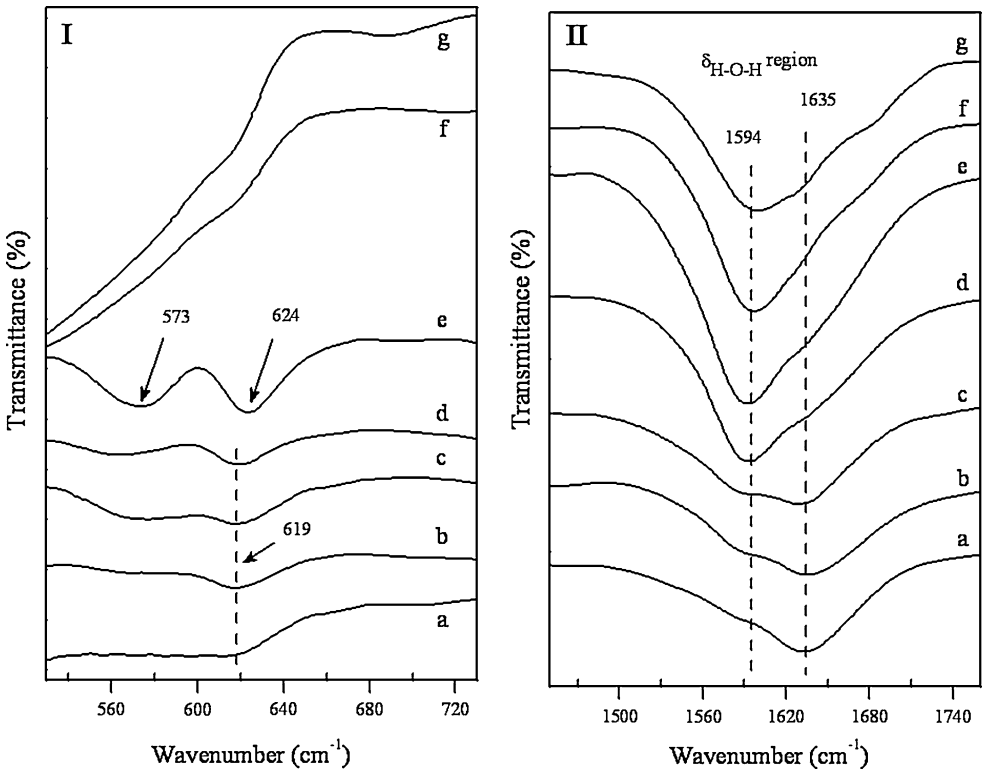

Fig. 12 FTIR spectra of SBA-15 and Cr-modified SBA-15 samples: *a* SBA-15-c, *b* Cr/Si(0.01)/SBA-15-c, *c* Cr/Si(0.05)/SBA-15-c, *d* CrO_x-imp/SBA-15-c, *e* CrO_x-poly/SBA-15-c, *f* $Cr(OH)_3$, *g* Cr_2O_3; samples *a–c* calcined at 550 °C and *d*, *e* and *g* calcined at 400 °C

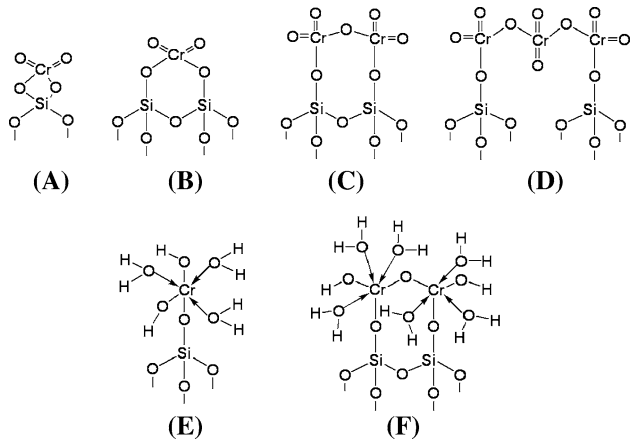

Fig. 13 Molecular chromium species grafted on SBA-15: isolated Cr-species attached to geminal silanol groups (**a**), and single silanol groups (**b**); dehydrated CrO_x dimer (**c**) and trimer (**d**) on single silanol groups; hydrated Cr^{3+} species (**e**) and (**f**)

SBA-15 walls and isolated CrO_x species attached to these walls. The broad NH_3 desorption features above 450 °C and centered around 507 and 588 °C, in addition to the weak features at 244 and 458 °C, are attributed to chromia clusters present on CrO_x/SBA-15 samples. The growth of chromia clusters appears to be significant on samples prepared by impregnation methods (spectra d and e) than by one-pot synthesis method. Chromia clusters can offer surface Lewis acid sites such as Cr^{6+} and Cr^{3+} ions where NH_3 can coordinate and desorb. This study can broadly distinguish between the Brønsted acidic sites (Si–OH) and Lewis acid sites (Cr^{6+}/Cr^{3+}) on CrO_x/SBA-15 samples prepared by Cr-polycation sol and other approaches.

4 Conclusions

Chromia species grafted on mesoporous SBA-15 by various methods including Cr-polycation sol precursor have been analyzed. The Cr^{3+} and Cr-polycation solutions are also studied by UV–Vis spectroscopy. The blue aqueous Cr^{3+} shows there absorption bands at 296, 409 and 575 nm. The green Cr-polycation shows only two absorption bands at 419 and 580 nm. Analysis of CrO_x/SBA-15 samples obtained by one-pot synthesis approach shows isolated CrO_x species in the submonolayer regime essentially containing Cr^{6+} species. These species are not detectable in PXRD but show $O^{2-} \rightarrow Cr^{6+}$ charge transfer transition in UV-Vis DRS. They undergo reduction below 410 °C in H_2-TPR. The bulk-like hydrated Cr_2O_3 clusters formed by Cr-polycation as well as direct impregnation method are reduced above 410 °C in H_2-TPR. The one-pot method seems to induce spherical as well as hexagonal morphologies of SBA-15 when Cr/Si ratio is 0.01. The final samples obtained by using $Cr(NO_3)_3$ and Cr-polycations as precursor solutions show transitions related to Cr^{3+} and Cr^{6+} ions. The polycation sample shows additional band at 605 nm due to the octahedrally coordinated Cr^{3+} in Cr_2O_3

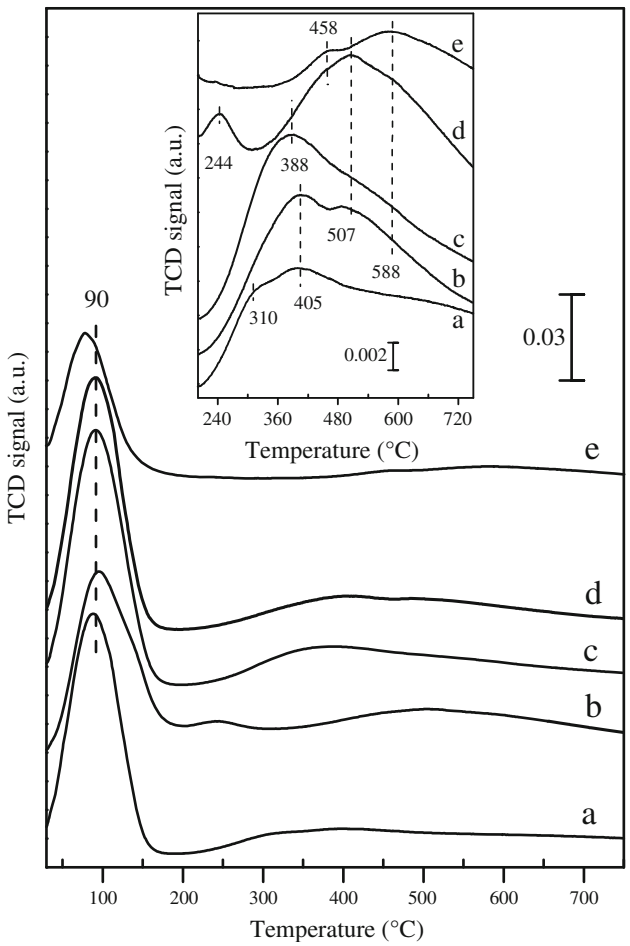

Fig. 14 NH_3-TPD profiles of SBA-15 and Cr-modified SBA-15 calcined samples: *a* SBA-15-c, *b* Cr/Si(0.01)/SBA-15-c, *c* Cr/Si(0.05)/SBA-15-c, *d* CrO_x-imp/SBA-15-c, *e* CrO_x-poly/SBA-15-c

clusters indicating different Cr^{3+}/Cr^{6+} ratio. This is also corroborated by the H_2-TPR experiments. One-pot synthesized samples predominantly contain Si–OH groups (1,635 cm^{-1}) while impregnated samples show –OH groups associated with CrO_x species (1,594 cm^{-1}) in the δ_{HOH} region, distinguishing the water molecules associated with silica surface and chromia clusters. The unique IR features at 573 and 624 cm^{-1} have been identified due to the extra-framework CrO_x species, exclusively obtained in the case of Cr-polycation precursor sample. NH_3-TPD spectra show strong desorption of physisorbed NH_3 around 90 °C from silanol groups of SBA-15, and almost negligible but measurable NH_3 desorption above 200 °C essentially from the chromia species present on SBA-15.

Acknowledgments Financial support from DRDO, New Delhi, through Grant ERIP/ER/0600319/M/01/1052 is gratefully acknowledged. We thank SERC division of DST, Ministry of Science and Technology, New Delhi, for providing powder XRD, TGA, TPR/TPD and BET facilities (under FIST Schemes). We also thank Mr. A. Narayanan and Mrs. S. Srividya for data collection using these facilities.

References

1. D. Zhao, Q. Huo, J. Feng, B.F. Chmelka, G.D. Stucky, J. Am. Chem. Soc. **120**, 6024 (1998)
2. C. Yu, B. Tian, X. Liu, J. Fan, H. Yang, D.Y. Zhao, in *Nanoporous Materials—Science and Engineering*, ed. by G.Q. Lu, X.S. Zhao (Imperial College Press, London, 2004), p. 14
3. L. Chmielarz, P. Kuśtrowski, M. Kruszec, R. Dziembaj, P. Cool, E.F. Vansant, J. Porous Mater. **12**, 183 (2005)
4. D. Srinivas, L. Saikia, Catal. Surv. Asia **12**, 114 (2008)
5. L. Zhang, Y. Zhao, H. Dai, H. He, C.T. Au, Catal. Today **131**, 42 (2008)
6. H. Xia, C. Zhou, D.S. Tong, C.X. Lin, J. Porous Mater. **17**, 225 (2010)
7. J. van der Meer, I. Bardez-Giboire, C. Mercier, B. Revel, A. Davidson, R. Denoyel, J. Phys. Chem. C **114**, 3507 (2010)
8. K. Zhu, B. Yue, W. Zhou, H. He, Chem. Commun. 98 (2003)
9. B.L. Newalkar, J. Olanrewaju, S. Komarneni, Chem. Mater. **13**, 552 (2001)
10. X. Xu, H. Xu, F. Kapteijn, J.A. Moulijn, Appl. Catal. B: Environ. **53**, 265 (2004)
11. G. Chen, Y. Zheng, X. Zheng, X. Shen, Y. Zheng, J. Porous Mater. **16**, 361 (2009)
12. W. Liu, S.Y. Lai, H. Dai, S. Wang, H. Sun, C.T. Au, Catal. Lett. **113**, 147 (2007)
13. Z. Huang, W. Bensch, W. Sigle, P.A. van Aken, L. Kienle, T. Vitoya, H. Modrow, T. Ressler, J. Mater. Sci. **43**, 244 (2008)
14. J. Sauer, F. Marlow, B. Spliethoff, F. Schuth, Chem. Mater. **14**, 217 (2002)
15. L. Saikia, D. Srinivas, P. Ratnasamy, Appl. Catal. A: Gen. **309**, 144 (2006)
16. Y. Wang, X. Wang, Z. Su, Q. Guo, Q. Tang, Q. Zhang, H. Wan, Catal. Today **93–95**, 155 (2004)
17. D. Srinivas, P. Ratnasamy, Micropor. Mesopor. Mater. **105**, 170 (2007)
18. S. Huh, J.W. Wiench, J.-C. Yoo, M. Pruski, V.S-Y. Lin, Chem. Mater. **15**, 4247 (2003)
19. C. Yu, J. Fan, B. Tian, D. Zhao, Chem. Mater. **16**, 889 (2004)
20. B.M. Weckhuysen, I.E. Wachs, R.A. Schoonheydt, Chem. Rev. **96**, 3327 (1996)
21. X. Shi, S. Ji, K. Wang, Catal. Lett. **125**, 331 (2008)
22. W. Zhang, T.J. Pinnavaia, Catal. Lett. **38**, 261 (1996)
23. S. Shylesh, P.P. Samuel, A.P. Singh, Appl. Catal. A: Gen. **318**, 128 (2007)
24. M.P. McDaniel, J. Catal. **67**, 71 (1981)
25. X. Zhang, Y. Yue, Z. Gao, Catal. Lett. **83**, 19 (2002)
26. K.A. Carrado, S.L. Suib, N.D. Skoularikis, R.W. Coughlin, Inorg. Chem. **25**, 4217 (1986)
27. R.M. Carr, Clays Clay Miner. **33**, 357 (1985)
28. R. Toranzo, M.A. Vicente, M.A. Bañares-Muñoz, Chem. Mater. **9**, 1829 (1997)
29. T.J. Pinnavaia, M. Tzou, S.D. Landau, J. Am. Chem. Soc. **107**, 4783 (1985)
30. G. Mata, R. Trujillano, M.A. Vicente, C. Belver, M. Fernández-García, S.A. Korili, A. Gil, Appl. Catal. A: Gen. **327**, 1 (2007)
31. B.G. Mishra, G. Ranga Rao, Micropor. Mesopor. Mater. **70**, 43 (2004)
32. B.G. Mishra, G. Ranga Rao, J. Porous Mater. **12**, 171 (2005)
33. H. Stünzi, W. Marty, Inorg. Chem. **22**, 2145 (1983)
34. D. Zhao, J. Sun, Q. Li, G.D. Stucky, Chem. Mater. **12**, 275 (2000)
35. G. Wang, L. Zhang, J. Deng, H. Dai, H. He, C.T. Au, Appl. Catal. A: Gen. **355**, 192 (2009)
36. M. Kruk, M. Jaroniec, C.H. Ko, R. Ryoo, Chem. Mater. **12**, 1961 (2000)
37. B.M. Weckbuysen, L.M.D. Ridder, R.A. Schoonheydt, J. Phys. Chem. **97**, 4156 (1993)

38. B. Fubini, G. Ghiotti, L. Stradella, P. Garrone, C. Morterra, J. Catal. **66**, 200 (1980)
39. A. Sakthivel, P. Selvam, J. Catal. **211**, 134 (2002)
40. R.A. Schoonheydt, Chem. Soc. Rev. **39**, 5051 (2010)
41. B.M. Weckhuysen, A.A. Verberckmoes, A.R.D. Baets, R.A. Schoonheydt, J. Catal. **166**, 160 (1997)
42. M. Mägi, E. Lippmaa, A. Samoson, G. Engelhardt, A.-R. Grimmer, J. Phys. Chem. **88**, 1518 (1984)
43. Y. Xia, H. Dai, H. Jiang, J. Deng, H. He, C.T. Au, Environ. Sci. Technol. **43**, 8355 (2009)
44. X. Zhao, X. Wang, J. Mol. Catal. A: Chem. **261**, 225 (2007)
45. M. Cherian, M.S. Rao, A.M. Hirt, I.E. Wachs, G. Deo, J. Catal. **211**, 482 (2002)
46. V. Ramaswamy, P. Shah, K. Lazar, A.V. Ramaswamy, Catal. Surv. Asia **12**, 283 (2008)